Effect of Co and Fe stoichiometry on terahertz emission from Ta/(Co_{x}Fe_{1−x})_{80}B_{20}/MgO thin films

Yuta Sasaki, Yohei Kota, Satoshi Iihama, Kazuya Z. Suzuki, Akimasa Sakuma, and Shigemi Mizukami

Phys. Rev. B **100**, 140406 — Published 11 October 2019

DOI: 10.1103/PhysRevB.100.140406

Effect of Co and Fe stoichiometry on terahertz emission from $Ta/(Co_xFe_{1-x})_{80}B_{20}/MgO$ thin films

Yuta Sasaki,[1,2,*] Yohei Kota,[3] Satoshi Iihama,[2,4] Kazuya Z. Suzuki,[2,4] Akimasa Sakuma,[1,4,5] and Shigemi Mizukami[2,4,5,†]

[1] *Department of Applied Physics, Graduate School of Engineering, Tohoku University, Aoba 6-6-05, Sendai 980-8579, Japan*

[2] *WPI Advanced Institute for Materials Research, Tohoku University, Katahira 2-1-1, Sendai 980-8577, Japan*

[3] *National Institute of Technology, Fukushima College, Iwaki, Fukushima 970-8034, Japan*

[4] *Center for Spintronics Research Network (CSRN), Tohoku University, Sendai 980-8577, Japan*

[5] *Center for Science and Innovation in Spintronics (CSIS), Core Research Cluster (CRC), Tohoku University, Sendai 980-8577, Japan*

(Dated: September 30, 2019)

Abstract

Laser pulse-induced terahertz (THz) emission from Ta/$(Co_xFe_{1-x})_{80}B_{20}$/MgO thin films, with varying compositions x and annealing temperatures, is investigated. With increasing annealing temperature, the THz emission intensity exhibits significant dependence on x, with maxima at x of 0.1–0.3. The x dependence of the THz emission originated from the composition dependence of the spin currents induced in Co_xFe_{1-x} formed by the crystallization of amorphous CoFeB after the annealing. The origin of the laser-induced spin current is qualitatively discussed in terms of a ballistic transport of hot electrons and a spin-dependent Seebeck effect with different compositions.

Laser pulse-induced terahertz (THz) emission from ferromagnetic (FM) and nonmagnetic heavy metal (NHM) bilayers has been attracting increasing attention. Kampfrath *et al.* first discussed the underlying physics [1], namely the superdiffusive spin current pulse is induced by a laser pulse [2, 3], then the spin current pulse is converted to the charge current pulse via the inverse spin-Hall effect [4, 5], and finally the charge current pulse emits the THz electromagnetic pulse. The inverse Rashba-Edelstein effect was also discussed as a spin-charge conversion route in a THz emission observed in CoFeB/Ag/Bi trilayers [6]. A helicity-dependent THz emission related to the optical spin-torque was also investigated in FM/NHM bilayers [7]. Among them, the inverse-spin Hall effect-based THz emission has been mostly studied from both fundamental and technological points of view [8–22].

Seifert *et al.* experimentally demonstrated the systematic NHM dependence of the laser-induced THz emission intensity in FM/NHM bilayers, and they also reported that those dependences were consistent with the NHM dependences of the theoretical spin-Hall conductivity [8]. They also investigated FM dependence of the laser-induced THz emission intensity in FM/NHM bilayers [8, 14]. For their data, CoFeB exhibited much more intense THz emission as compared with Fe, Co, and Ni. Although they discussed this FM dependence in terms of the difference of magnetic transition temperatures [8], spin polarization of FM, and interface properties [14], it is not yet clear how the spin current magnitude and resulting THz emissions depend on FM.

We previously reported that laser-induced THz emission intensity in Ta/CoFeB/MgO structures was significantly increased by annealing the samples [13]. This was considered as

* SASAKI.Yuta@nims.go.jp

† shigemi.mizukami.a7@tohoku.ac.jp

a result of the enhancement of the spin-dependent mean free path in CoFeB, by a crystallization of an amorphous CoFeB into (001)-oriented crystalline bcc CoFe, in the annealing process [13]. In this study, we report—for the first time—observation of the systematic change in the THz emission from Ta/CoFeB/MgO structures with varying composition ratios for the magnetic elements, Co and Fe. The THz emission was enhanced at certain compositions, at which the saturation magnetization shows a maximum. The observed dependences reflect the composition dependence of the laser-induced spin current, and the physical origin is discussed.

The films were deposited on thermally-oxidized Si substrates using a magnetron sputtering technique. The multilayer stacking structure was substrate/ Ta (5)/ $(Co_xFe_{1-x})_{80}B_{20}$ (4)/ MgO (2)/ Ta (2) (thickness in nm). Here, a bottom and top Ta layer serve as the spin-charge converter and a protective layer, respectively. MgO promotes the crystallization of CoFeB into (001)-oriented CoFe during the sample annealing [23, 24]. A co-sputtering method using $Co_{80}B_{20}$ and $Fe_{80}B_{20}$ targets were employed to vary a nominal Co concentration $x = 0 - 0.75$. Each sample with different x were cut into several pieces, and each piece was annealed at different temperature T_a of $300 - 450$°C, for 1 h in a vacuum furnace. The crystalline structures and magnetic properties of the samples were characterized using X-ray diffraction (XRD) and a vibrating sample magnetometer (VSM), respectively. The sheet conductance for the films was measured by a standard four probe method. The laser-induced THz emission was measured using a standard optical set-up in air [13]. A Ti:sapphire laser and regenerative amplifier were used as a light source. The pulse duration, center wavelength, and repetition rate for the output laser were approximately 120 fs, 800 nm, and 1 kHz, respectively. The pump laser was focused on the film surface at normal incidence and its fluence per pulse was 0.7 mJ/cm^2. The THz wave, emitted from the films, was collimated using a parabolic mirror and focused onto a 1-mm-thick ZnTe (110) crystal with another parabolic mirror. The THz wave intensity was measured, via an electro-optic effect, for a probe laser passing through the ZnTe crystal [25–27]. An in-plane magnetic field was applied to the samples using an electromagnet with a maximum field of 2 T. The detail of the measurement is described in Ref. [13].

First, we briefly note the theoretical background of the THz emission in FM/NHM [8]. A THz electric field $\mathbf{E}$ at the outer surface of the film, generated by the laser pulse induced spin current J_s across the FM/NHM interface, is expressed as the relation in a frequency ω

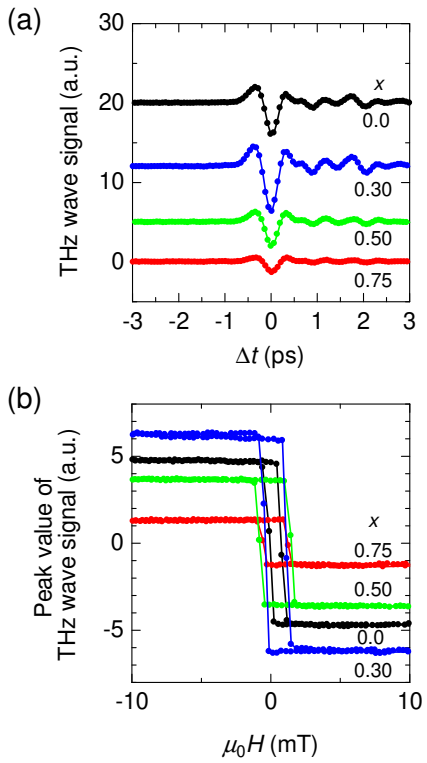

FIG. 1. (a) The THz time-domain signals for Ta/$(Co_xFe_{1-x})_{80}B_{20}$/MgO samples with different x. The samples shown here were annealed at 400°C and an in-plane magnetic field $\mu_0 H$ of 100 mT was applied. (b) The magnetic field-swept THz signals at zero time delay for the same samples.

domain [8]:

$$\mathbf{E}(\omega) = Z(\omega)\Lambda_{\rm s}\theta_{\rm s}\frac{e}{\hbar}J_{\rm s}(\omega)\mathbf{n}\times\mathbf{m}, \tag{1}$$

where $\mathbf{n}$ and $\mathbf{m}$ are a normal vector and magnetization unit vector, respectively. θ_s and Λ_s are the spin-Hall angle and spin relaxation length, respectively, in NHM for carriers relevant to $J_{\rm s}$. Z is the electromagnetic impedance [8]:

$$1/Z(\omega) = \left[n_0 + n_{\rm s}(\omega)\right]/Z_0 + G_{\rm s}(\omega). \tag{2}$$

Here, $n_{0(s)}$ is the refractive index for air (substrate) and Z_0 is the vacuum impedance. G_s is the sheet conductance for the sample films and is defined as $G_{\rm s} = \sum_i \sigma_i(\omega)d_i$, where $\sigma_i(\omega)$ and d_i are the ac conductivity and thickness for the i-th metallic layer, respectively. Equations (1) and (2) assume, respectively, that the NHM layer is thicker than $\Lambda_{\rm s}$ and the total film thickness is smaller than the wavelength of the THz wave [8]. In the present set-up,

the electric field of the detected THz wave is regarded as a far field that is approximately related to the time derivative of $\mathbf{E}$ [28].

The representative data of the THz emission are illustrated in Fig. 1. Figure 1(a) displays the electric field of the THz wave for the $T_a = 400$°C films with different compositions x, recorded in the time domain. The data were recorded with an in-plane magnetic field of 100 mT. For convenience, here we define the zero time delay in Fig. 1(a) as the dip position of the THz signals. As seen in the figure, although those intensities are remarkably different against the compositions, the shape of the signals exhibit negligible changes with different compositions. This implies that the functional dependences of the physical quantities on ω in Eqs. (1) and (2) are approximately the same in the present measurement bandwidth, and only those magnitudes are varied among the samples. We also measured the magnetic field-dependent THz emission for the samples. Figure 1(b) depicts the magnetic field-swept THz amplitude at zero time delay, for the samples illustrated in Fig. 1(a). The data observed here are very similar to the in-plane magnetization hysteresis curves for the samples (not shown here), being consistent with the proportionality of $\mathbf{E} \propto \mathbf{n} \times \mathbf{m}$ in Eq. (1).

Figure 2(a) depicts the composition dependence of the THz emission intensity at zero time delay for the samples annealed at various $T_{\rm a}$. For the as-deposited samples, the composition dependence is relatively weak and exhibit a broad maximum at x of about 0.3–0.4. The composition dependence becomes more remarkable with increasing $T_{\rm a}$, showing maxima at x values of 0.1–0.3. As seen in Eqs. (1) and (2), the sheet conductance $G_{\rm s}$ of the films affects the THz emission intensity. The typical dc data of $G_{\rm s}$ for the samples are shown in Fig. 2(b). The values for $G_{\rm s}$, for the as-deposited samples, are almost independent of the composition x. Though after annealing, G_s increases with increasing x. The trend of $G_{\rm s}$ is totally different from that of the THz emission. The $G_{\rm s}$ values for the metallic films at the frequency ($<\sim 1-2$ THz) in this study are considered to be similar to the dc values [8], and the properties in Ta, such as $\Lambda_{\rm s}$ and $\theta_{\rm s}$, would be independent of x. Therefore, we consider that the composition dependence of the THz emission after the annealing originates from that of the spin current $J_{\rm s}$, according to Eqs. (1) and (2).

Our previous report demonstrated that the laser-induced spin current $J_{\rm s}$ is closely related to the degree of the crystallization of CoFeB into (001)-oriented CoFe [13]. Thus, the composition dependence of the degree of crystallization was also verified with the XRD measurements, as shown in Fig. 3(a). Although it is difficult to clearly observe diffraction

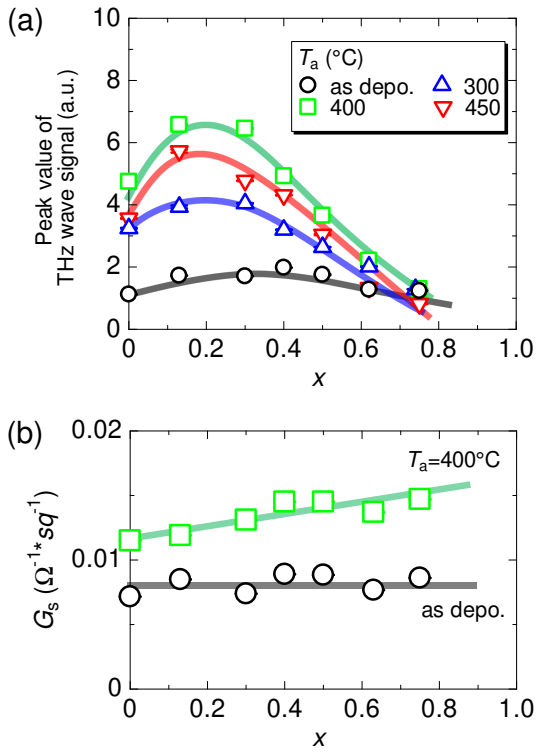

FIG. 2. (a) Peak values of the THz signals as a function of x for Ta/$(Co_xFe_{1-x})_{80}B_{20}$/MgO samples with different annealing temperatures T_a. (b) Typical data of the dc sheet conductance G_s as a function of x, for the as-deposited samples and the samples annealed at T_a of 400°C.

peaks for very thin polycrystalline textured CoFeB layers, the broad shoulders near the diffraction peak—due to the substrates—can be attributed to the bcc CoFe (002) diffraction peak. The data indicate that most of the films with different compositions are crystallized after the annealing at 400°C. The (002) diffraction peak is not detected for the $x = 0.75$ samples because the composition is close to that for the bcc-fcc phase boundary of the binary [29]. The degree of crystallization can be gained by an increase in the saturation magnetization M_s [30], as illustrated in Fig. 3(b). The annealing increases M_s for the samples with overall compositions due to the crystallization of CoFeB. In addition, the M_s values for the samples after the annealing are in agreement with those determined by the Slater-Pauling rule hold in CoFe alloys [31, 32]. Thus, we rule out the possibility that the remarkable composition effect on the THz emission (i.e. J_s), after the annealing, is caused by the compositional variation of the degree of crystallization.

Various induction processes of spin current J_s induced by a laser pulse have been consid-

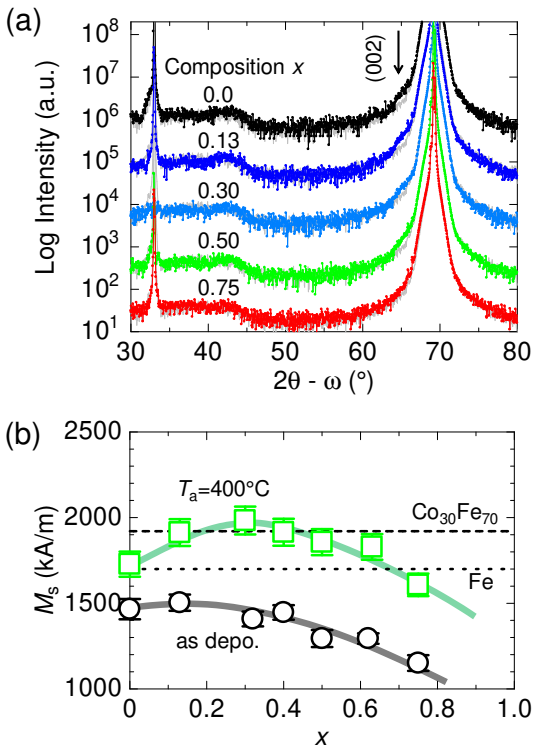

FIG. 3. (a) Typical XRD pattern for the Ta/$(Co_xFe_{1-x})_{80}B_{20}$/MgO samples annealed at 400°C with different compositions x. Thin curves are the data measured for the bare substrate, for comparison. The arrow indicates the typical position of the diffraction line for the bcc (002) for CoFe. (b) Typical data for the saturation magnetization M_s as a function of x, for the as-deposited samples and the samples annealed at T_a of 400°C.

ered. One well-known process is due to the transport of the laser-excited spin-polarized hot carriers. Such transport is roughly categorized into a ballistic and diffusive regime, before and after electron thermalization is achieved, and the superdiffusive regime as an intermediate case [2, 3]. For example, the non-thermal spin current, such as ballistic spin current, is launched for tens fs timescale. This may be characterized by the ballistic emission of the photo-exited carriers from FM into NHM [33, 34], but it is still a pure spin current without a charge current due to the dielectric screening characterized by the plasma frequency—which is much faster than the above mentioned timescale [2, 3, 33, 34]. Ballistic and superdiffusive spin current may be overlapped because of strong electron-electron interaction, and on this timescale, the transport and thermalization of laser-excited electrons are entangled [2, 3]. Typical diffusive spin current is driven by a thermal gradient, such as the spin-dependent

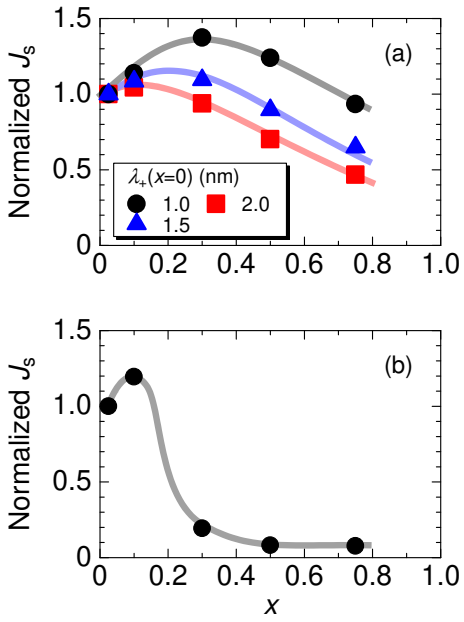

FIG. 4. Composition x dependence of the theoretically calculated spin current J_s as a souse of the THz emission in $Fe_{1-x}Co_x$ alloys. (a) The ballistic spin current evaluated with different mean free path for the up spin λ_+. (b) The diffusive spin current induced by the spin-dependent Seebeck effect. Curves are the visual guides.

Seebeck effect [14, 35].

We first discuss the spin current J_s in terms of the ballistic transport [33]. Here, we consider that J_s is carried by hot *sp* electrons created via an optical transition from *d* states and also take account of only the hot electrons near the Fermi level E_F, for simplicity. This is because the lifetimes for hot electrons rapidly decrease down to several fs with increasing electron energy, relative to E_F [36], which is much shorter than the pulse duration of ~ 120 fs in this study. Then, the J_s in FM at the FM/NHM interface may be roughly approximated by a difference in the spin-polarized current of the up (+) and down (-) *sp* electrons. Using those densities of states $N_\pm$ and taking account of those mean free path $\lambda_\pm$, the spin current can be approximately expressed as (see Supplemental Material [37]),

$$J_s \propto \sum_{\sigma=\pm} \sigma N_\sigma \lambda_\sigma \left[1 - \exp\left(-d_{FM}/\lambda_\sigma\right)\right]. \tag{3}$$

Here σ is a spin index. Figure 4(a) shows the value of J_s calculated using Eq. (3) for Co_xFe_{1-x} alloys. In this calculation, for simplicity, we consider only the hot *sp* electrons with velocities parallel to the [001] direction. Then, $N_\pm$ was approximated as the spin-dependent partial

density-of-states (DOS) of the Δ_1 band. This is because the electron effective mass for the Δ_1 band is much smaller than those for the other bands. The $N_\pm$ values were mostly taken from Ref. 38 (see Supplemental Material [37]). The values for $\lambda_\pm$ in Eq. (3) at different x were evaluated using the relation $\lambda_\pm^{-1} = cD_\pm$ with the total spin-dependent DOS $D_\pm$ for disordered Co_xFe_{1-x} alloys. The $D_\pm$ values were evaluated from the first principles [39] (see Supplemental Material [37]), and the proportional constant c was assumed to be independent of x and spin. Instead of varying c, we chosen the value of λ_+ at $x = 0$ as a free parameter to fix the value of c (see Supplemental Material [37]). For case of $\lambda_+ = 2.0$ nm in Fig. 4(a), J_s shows the maxima at $x = 0-0.1$. This maxima originates from the large spin asymmetry of the Δ_1 band at $x = 0 - 0.1$. This can be understood from the relation $J_s \propto (N_+ - N_-)$ obtained from Eq. (3) for case of λ_σ large enough. With decreasing λ_+, the composition x at which J_s shows the maxima increases. This change is due to the change of the spin asymmetry of the mean free path at $x = 0.2 - 0.3$ (see Supplemental Material [37]). The case of λ_+ =1.5 nm is similar to the data for the annealed samples in Fig. 2(a). This value of λ_+ =1.5 nm is consistent with the reported value for Fe [40]. Note that the composition dependence of the observed THz emission for the annealed samples is quite similar to that of the tunnel magnetoresistance (TMR) ratio observed in the (001)-oriented CoFe(B)/MgO MTJs [41, 42]. Furthermore, Andrieu *et al.* interpreted that the composition dependence of the TMR ratio is *partially* due to the composition dependence of the partial DOS for the Δ_1 band with their spectroscopic experiments and their *ab-initio* calculation [43].

Next, we consider the diffusive spin current in terms of spin-dependent Seebeck effect [35]. For this case, the following relation is expected [35, 44]:

$$J_s \propto S_s^{\rm eff} = (1 - P_c^2) S_s. \tag{4}$$

Here, $S_s^{\rm eff}$ is the effective spin-dependent Seebeck coefficient, P_c the spin polarization for the conductivity, and S_s the spin-dependent Seebeck coefficient [35, 44]. The theoretical values of J_s using Eq. (4) are also shown in Fig. 4(b). Those values were calculated with the energy-dependent conductivity σ_c for the up and down spin band for disordered Co_xFe_{1-x} alloys from first principles [39] (see Supplemental Material [37]). The composition dependences of J_s shows the maxima at $x \sim 0.1$, whereas J_s for $x \geqq 0.3$ is negligibly small. Thus, this theoretical data would not be accord with the THz emission data in Fig. 2(a). Note that the small J_s for $x \geqq 0.3$ in Fig. 4(b) is due to the high P_c of 0.8–0.9 calculated (see

Supplemental Material [37]), which is larger than the experimental P_c of 0.6–0.8 at $x = 0.5$ [45, 46]. Therefore, it will be necessary to obtain the experimental data of both P_c and S_s of the alloys for further discussion.

Regarding on the above-mentioned hot carrier transport, the number of the hot carriers excited by the laser light absorption may also be dependent on the electronic structure below and above E_F in reality, which should be considered based on more sophisticated theoretical model. Moreover, in addition to the above mentioned hot carrier spin current, other spin current created by thermal magnons were also discussed in some cases, even for insulating magnets [35, 47]. The comprehensive discussion is out of scope of this study, so that these will be investigated in future work.

In summary, the laser pulse-induced THz emission from the Ta/$(Co_xFe_{1-x})_{80}B_{20}$/MgO thin films was investigated. The samples with different x and annealing temperatures showed the systematic change in the THz emission intensity. We observed the THz emission maxima in the samples with x of approximately 0.1–0.3 after the annealing at 400°C. The study clearly demonstrated that the THz emission and J_s have an FM material dependence. The induction mechanism of the spin current in this study was qualitatively discussed in terms of the ballistic transport and the spin-dependent Seebeck effect.

Y.S. acknowledges the Graduate Program in Spintronics (GP-Spin) at Tohoku University. This work was partially supported by KAKENHI (Nos. 16H03846 and 26103004), CSRN, and CREST (No. JPMJCR17J5).

---

[1] T. Kampfrath, M. Battiato, P. Maldonado, G. Eilers, J. Notzold, S. Mahrlein, V. Zbarsky, F. Freimuth, Y. Mokrousov, S. Blugel, M. Wolf, I. Radu, P.M. Oppeneer, and M. Munzenberg, Nat. Nanotechnol. **8,** 256 (2013).

[2] M. Battiato, K. Carva, and P.M. Oppeneer, Phys. Rev. Lett. **105,** 027203 (2010).

[3] M. Battiato, K. Carva, and P.M. Oppeneer, Phys. Rev. B **86,** 024404 (2012).

[4] E. Saitoh, M. Ueda, H. Miyajima, and G. Tatara, Appl. Phys. Lett., **88,** 182509 (2006).

[5] T. Kimura, Y. Otani, T. Sato, S. Takahashi, and S. Maekawa, Phys. Rev. Lett. **98,** 249901 (2007).

[6] M.B. Jungfleisch, Q. Zhang, W. Zhang, J.E. Pearson, R.D. Schaller, H. Wen, A. Hoffmann,

Phys. Rev. Lett. **120,** 207207 (2018).

[7] T.J. Huisman, R.V. Mikhaylovskiy, J.D. Costa, F. Freimuth, E. Paz, J. Ventura, P.P. Freitas, S. Blugel, Y. Mokrousov, T. Rasing, A. V. Kimel, Nat. Nanotechnol. **11,** 455 (2016).

[8] T. Seifert, S. Jaiswal, U. Martens, J. Hannegan, L. Braun, P. Maldonado, F. Freimuth, A. Kronenberg, J. Henrizi, I. Radu, E. Beaurepaire, Y. Mokrousov, P.M. Oppeneer, M. Jourdan, G. Jakob, D. Turchinovich, L.M. Hayden, M. Wolf, M. Mnzenberg, M. Klui, and T. Kampfrath, Nat. Photonics **10,** 483 (2016).

[9] D. Yang, J. Liang, C. Zhou, L. Sun, R. Zheng, S. Luo, Y. Wu, and J. Qi, Adv. Opt. Mater. **4,** 1944 (2016).

[10] T.J. Huisman, C. Ciccarelli, A. Tsukamoto, R. V. Mikhaylovskiy, T. Rasing, and A. V. Kimel, Appl. Phys. Lett. **110,** 072402 (2017).

[11] T. Seifert, S. Jaiswal, M. Sajadi, G. Jakob, S. Winnerl, M. Wolf, M. Klui, and T. Kampfrath, Appl. Phys. Lett. **110,** 252402 (2017).

[12] Y. Wu, M. Elyasi, X. Qiu, M. Chen, Y. Liu, L. Ke, and H. Yang, Adv. Mater. **29,** 1603031 (2017).

[13] Y. Sasaki, K.Z. Suzuki, and S. Mizukami, Appl. Phys. Lett. **111,** 102401 (2017).

[14] T. Seifert, U. Martens, S. Gnther, M.A.W. Schoen, F. Radu, X.Z. Chen, I. Lucas, R. Ramos, M.H. Aguirre, P.A. Algarabel, A. Anadn, H.S. Krner, J. Walowski, C. Back, M.R. Ibarra, L. Morelln, E. Saitoh, M. Wolf, C. Song, K. Uchida, M. Mnzenberg, I. Radu, and T. Kampfrath, Spin **7,** 1740010 (2017).

[15] G. Torosyan, S. Keller, L. Scheuer, R. Beigang, and E.T. Papaioannou, Sci. Rep. **8,** 1311 (2018).

[16] T.S. Seifert, N.M. Tran, O. Gueckstock, S.M. Rouzegar, L. Nadvornik, S. Jaiswal, G. Jakob, V. V. Temnov, M. Munzenberg, M. Wolf, M. Klaui, and T. Kampfrath, J. Phys. D. Appl. Phys. **51,** 364003 (2018).

[17] G. Li, R.V. Mikhaylovskiy, K.A. Grishunin, J.D. Costa, T. Rasing, A.V. Kimel, J. Phys. D. Appl. Phys. **51,** 134001 (2018).

[18] H.S. Qiu, K. Kato, K. Hirota, N. Sarukura, M. Yoshimura, and M. Nakajima, Opt. Express **26,** 15247 (2018).

[19] H. Qiu, L. Wang, Z. Shen, K. Kato, N. Sarukura, M. Yoshimura, W. Hu, Y. Lu, and M. Nakajima, Appl. Phys. Express **11,** 092101 (2018).

[20] S. Zhang, Z. Jin, Z. Zhu, W. Zhu, Z. Zhang, G. Ma, and J. Yao, J. Phys. D. Appl. Phys. **51,** 034001 (2018).

[21] R. Schneider, M. Fix, R. Heming, S. Michaelis de Vasconcellos, M. Albrecht, R. Bratschitsch, ACS Photonics. **5,** 3936 (2018).

[22] M. Chen, R. Mishra, Y. Wu, K. Lee, H. Yang, Adv. Opt. Mater. **6,** 1800430 (2018).

[23] D.D. Djayaprawira, K. Tsunekawa, M. Nagai, H. Maehara, S. Yamagata, N. Watanabe, S. Yuasa, Y. Suzuki, and K. Ando, Appl. Phys. Lett. **86,** 092502 (2005).

[24] S. Yuasa, Y. Suzuki, T. Katayama, and K. Ando, Appl. Phys. Lett. **87,** 242503 (2005).

[25] A. Nahata, A.S. Weling, and T.F. Heinz, Appl. Phys. Lett. **69,** 2321 (1996).

[26] Q. Wu and X.-C. Zhang, Appl. Phys. Lett. **71,** 1285 (1997).

[27] G. Gallot and D. Grischkowsky, J. Opt. Soc. Am. B **16,** 1204 (1999).

[28] A. Gurtler, C. Winnewisser, H. Helm, and P. Uhd Jepsen, J. Opt. Soc. Am. A **17,** 74 (2000).

[29] I. Ohnuma, H. Enoki, O. Ikeda, R. Kainuma, H. Ohtani, B. Sundman, and K. Ishida, Acta Mater. **50,** 379 (2002).

[30] J.P. Pellegren and V.M. Sokalski, IEEE Trans. Magn. **51,** 1 (2015).

[31] Ferromagnetism, by Richard M. Bozorth, pp. 992. ISBN 0-7803-1032-2. Wiley-VCH , August 1993.

[32] D.I. Bardos, J. Appl. Phys. **40,** 1371 (1969).

[33] A. Melnikov, I. Razdolski, T.O. Wehling, E.T. Papaioannou, V. Roddatis, P. Fumagalli, O. Aktsipetrov, A.I. Lichtenstein, and U. Bovensiepen, Phys. Rev. Lett. **107,** 076601 (2011).

[34] A. Alekhin, I. Razdolski, N. Ilin, J.P. Meyburg, D. Diesing, V. Roddatis, I. Rungger, M. Stamenova, S. Sanvito, U. Bovensiepen, and A. Melnikov, Phys. Rev. Lett. **119,** 017202 (2017).

[35] G.-M. Choi, C.-H. Moon, B.-C. Min, K.-J. Lee, and D.G. Cahill, Nat. Phys. **11,** 576 (2015).

[36] V.P. Zhukov, E.V. Chulkov, and P.M. Echenique, Phys. Rev. B **73,** 125105 (2006).

[37] See Supplemental Material at [URL will be inserted by publisher] for details of the theoretical calculations.

[38] B. Belhadji and L. Calmels, Phys. Rev. B **83,** 092401 (2011).

[39] Y. Kota, T. Takahashi, H. Tsuchiura, and A. Sakuma, J. Appl. Phys. **105,** 07B716 (2009).

[40] B. A. Gurney, V. S. Speriosu, J.-P. Nozieres, H. Lefakis, D. R. Wilhoit, and O. U. Need, Phys. Rev. Lett. **71**, 4023 (1993).

[41] Y.M. Lee, J. Hayakawa, S. Ikeda, F. Matsukura, and H. Ohno, Appl. Phys. Lett. **90,** 212507 (2007).

[42] F. Bonell, T. Hauet, S. Andrieu, F. Bertran, P. Le Fvre, L. Calmels, A. Tejeda, F. Montaigne, B. Warot-Fonrose, B. Belhadji, A. Nicolaou, and A. Taleb-Ibrahimi, Phys. Rev. Lett. **108,** 176602 (2012).

[43] S. Andrieu, L. Calmels, T. Hauet, F. Bonell, P. Le Fvre, and F. Bertran, Phys. Rev. B **90,** 214406 (2014).

[44] A. Slachter, F.L. Bakker, J.-P. Adam, and B.J. van Wees, Nat. Phys. **6,** 879 (2010).

[45] H. Yuasa, M. Yoshikawa, Y. Kamiguchi, K. Koi, H. Iwasaki, M. Takagishi, and M. Sahashi, J. Appl. Phys. **92,** 2646 (2002).

[46] T. Mano, I. C. Chu, K. Miyake, M. Doi, S. Kuwano, T. Shima, and M. Sahashi, IEEE Trans. Magn. **45,** 3460 (2009).

[47] T.S. Seifert, S. Jaiswal, J. Barker, S.T. Weber, I. Razdolski, J. Cramer, O. Gueckstock, S.F. Maehrlein, L. Nadvornik, S. Watanabe, C. Ciccarelli, A. Melnikov, G. Jakob, M. Munzenberg, S.T.B. Goennenwein, G. Woltersdorf, B. Rethfeld, P.W. Brouwer, M. Wolf, M. Klaui, and T. Kampfrath, Nat. Commun. **9,** 2899 (2018).